

Research Article

Growth Kinetics and Sensing Features of Colloidal Silver Nanoplates

Giuseppe Compagnini¹,¹ Marcello Condorelli,¹ Maria E. Fragalà,¹ Vittorio Scardaci,¹ Ilaria Tinnirello,¹ Orazio Puglisi,¹ Fortunato Neri,² and Enza Fazio²

¹Dipartimento di Scienze Chimiche, Università di Catania, Viale A. Doria 6, Catania 95125, Italy

²Dipartimento di Scienze Matematiche e Informatiche, Scienze Fisiche e Scienze della Terra, Università di Messina, Messina, Italy

Correspondence should be addressed to Giuseppe Compagnini; gcompagnini@unict.it

Received 29 July 2018; Revised 10 October 2018; Accepted 28 October 2018; Published 15 January 2019

Academic Editor: William Yu

Copyright © 2019 Giuseppe Compagnini et al. This is an open access article distributed under the Creative Commons Attribution License, which permits unrestricted use, distribution, and reproduction in any medium, provided the original work is properly cited.

This paper presents the growth mechanisms and the plasmon sensing features for a large class of silver nanoplates obtained in the colloidal form. The synthesis is conducted by seed-mediated growth and leads to plates with aspect ratios as large as 20, having localized surface plasmon resonances extending deeply into the infrared spectral region (1000 nm and above). We measure plasmon sensitivity by varying the colloidal local refractive index, and $\Delta\lambda/\Delta n$ sensitivity values up to 500 nm/RIU are obtained. Theoretical considerations regarding the correlation between the refractive index sensitivity and the position of the main localized plasmon resonance band demonstrate that plasmon sensitivity does not depend directly on the nanoparticle shape and aspect ratio.

1. Introduction

1.1. Metal Nanoparticles for Sensing. Metal nanoparticles catalyzed a large research interest because of their applications in several fields such as photonics, electronics, catalysis, sensing, and biological labeling [1–3]. One of the most important features of this kind of nanostructures is interacting with an external electromagnetic field through their conduction electrons, exciting plasmon resonances [4]. The plasmonic behavior of a metal nanoparticle depends on the composition (e.g., the dielectric functions of the material), on the refractive index of the surrounding medium and on several geometrical features, such as shape and size. In a collection of particles, the resonance frequencies are also driven by their spatial arrangements including the distance between them [5–7]. All these facts contribute to determining the quality of nanoparticle response towards a large number of phenomena such as enhanced spectroscopic signals [8–10] or enhanced catalysis [11–13]. In advanced sensing applications, a highly localized field induced by plasmon resonance excitations makes metal nanostructures sensitive probes to

detect local variations in the surrounding environment at a molecular level. For example, local changes in the refractive index, due to adsorption of proteins or biomolecules onto the nanoparticle's surface, can be easily detected by spectral changes. For these reasons, nanoplasmonic sensing is emerging as a simple and extremely sensitive strategy for real-time detection of biological or chemical interactions and it is also suitable for device miniaturization and multiplexing due to the small dimensions of metal nanoparticles [14, 15].

1.2. Seed-Mediated Approach for Nanoparticle Growth. In the last decade, different approaches to produce gold and silver nanoparticles with different plasmonic features have been developed [11, 16, 17]. One of the most used is the so-called “seed-mediated growth” method [18] which is recognized as an easy, straightforward, and low-cost strategy, also suitable for scale up production. The optimization of any synthetic protocol is a fundamental step for tailoring the shapes and sizes of noble metal particles as it gives the possibility to act on a temporal separation of the nucleation and growth stages. In fact, the basics of the seed-assisted

generation of silver nanoplates regard the ability to drive silver nanoplatelet growth onto preexisting seeds, thus disfavoring homonucleation events [19]. Different parameters such as seed concentration, nature and concentration of surfactants, nature and concentration of impurities and additives, growth temperature, growth time, and pH values determine the final colloidal features. Herein, in the frame of a seed-mediated growth procedure, we investigate the role played by the reactant addition rate and the concentration of seeds in order to control silver nanoplate aspect ratio and shape. Once we have obtained a range of different colloidal samples having plasmon resonances from near UV (below 400 nm) to near IR (above 1000 nm), we have verified their specific sensing features in terms of refractive index sensitivity, as the dielectric constant of the surrounding medium varies. We have also compared these sensitivities with an analytical model which, up to now, has been tested only computationally.

2. Materials and Methods

2.1. Silver Nanoparticle Preparation. Silver nitrate (AgNO_3 , 99.9%), tri-sodium citrate (TSC, 99%), sodium borohydride (NaBH_4 , 99%), and hydrated hydrazine (50–60%) have been purchased from Sigma-Aldrich and used as received without further treatment. Deionized water ($>18.4 \text{ M}\Omega\cdot\text{cm}$) was used in all of the synthesis processes. Silver seed solution is obtained by reducing a silver nitrate solution by using sodium borohydride ($E_0 = -0.78 \text{ V}$), in the presence of TSC as a stabilizing agent. In particular, we added 0.5 mL of a 20 mM NaBH_4 solution to 10 mL of a 59 mM AgNO_3 one, in the presence of TSC (1 mL, 35 mM). The reaction is conducted at $293 \pm 1 \text{ K}$ under strong stirring. The as-prepared colloid was then aged for 24 hours before use to ensure a complete reduction of AgNO_3 .

Defined aliquots of colloidal seeds, ranging from $20 \mu\text{L}$ to 1 mL ($\pm 1 \mu\text{L}$), are mixed with a freshly prepared 20 mL solution of hydrated hydrazine ($\text{N}_2\text{H}_4\cdot 2\text{H}_2\text{O}$) and TSC. Each of these former colloids is a reactor (solution A) for the growth of specific silver nanoplates. From here on, a 59 mM solution of AgNO_3 (solution B) is added dropwise to solution A, by varying the addition rate from 0.1 mL/min to 10 mL/min. The addition rate has been controlled by using a peristaltic pump with an error below 0.01 mL/min. All the experiments have been performed at $293 \pm 1 \text{ K}$ in a thermostatically controlled room. The obtained colloidal dispersions have colors which change from yellow to orange, pink, red, green, and finally to blue (Figure 1), according to the shape and size of the nanoplates (from here on AgNPTs). The blue color corresponds to the biggest AgNPTs.

2.2. Characterization Methods. Once the colloid has been produced, a range of spectroscopic and morphologic characterizations has been performed. Some of them involve the colloid itself, and others have been performed after the deposition of some drops of the colloid under investigation onto a suitable surface (flat and conductive). In particular, extinction spectra have been obtained in the range 250–1100 nm using an Agilent Cary 60 UV-Vis spectrophotometer. A fraction of the colloids was deposited on nickel grids to carry out



FIGURE 1: Some of the colloidal dispersions obtained. Different colors correspond to different plasmon resonance features.

scanning transmission electron microscopy (STEM) characterization. STEM images were taken by a scanning electron microscope (ZEISS; model Merlin Gemini 2) operating at an accelerating voltage of 30 kV and at a working distance of 4 mm. AFM analyses have been performed using a WITec alpha300 RS machine in contact mode. Plasmon sensing has been evaluated by varying the refractive index of the medium through the addition of specific sucrose solution aliquots to the initial colloidal suspension (1.33–1.46 in refractive index units (RIU)).

3. Results and Discussion

3.1. Growth of Silver Nanoplates. In principle, the optical response of spherical silver colloids is predicted by Mie theory [18]. This theory defines a critical size for controlling the plasmon signal: for silver nanoparticles (in water), this limit is $\sim 50 \text{ nm}$ in diameter. Below this value, the applied optical field is uniform across the width of the nanoparticle and free electrons move as a single-electron cloud in resonance with light [20]. This condition is spectroscopically indicated by the appearance of characteristic plasmon resonance peaks whose wavelength is independent from the particle diameter. For particles larger than this critical size, however, the applied optical electric field begins to vary substantially in magnitude and phase from one end of the particle to the other. The electron cloud no longer oscillates as a single dipole unit. Consequently, the dipole peak shifts to longer wavelengths while quadrupole and octupole peaks begin to emerge at higher energies. Plasmon resonances change significantly moving from spherically to anisotropically shaped particles. The Mie theory and its extension to ellipsoids (Mie-Gans) fail to predict the plasmonic spectra. Accordingly, a number of computational approaches must be used and can be found in literature to model the optical response [21]. Typical extinction spectra of colloidal aqueous solutions containing spherical silver seeds (diameters below 40 nm) and silver nanoplates (AgNPTs) are reported in Figure 2.

Besides interband transition signals located below 300 nm, the resonance spectra of spherical nanoparticles and those of platelets deeply differ. The former has single sharp resonances at around 395 nm (red line) while the latter presents many plasmon modes which are generally attributed to the following [20]:

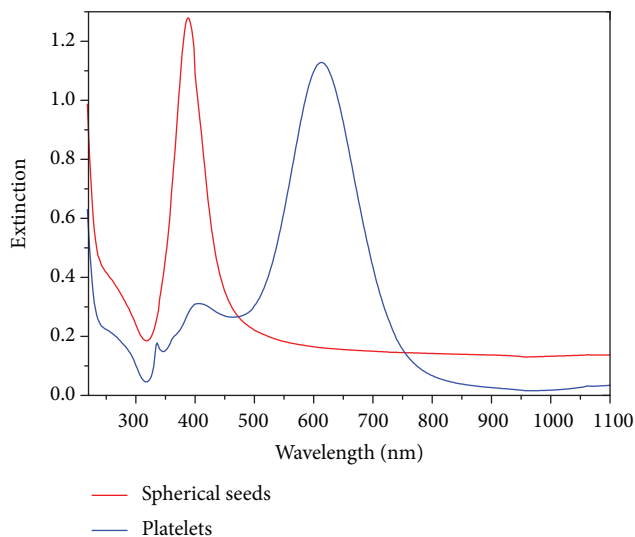


FIGURE 2: Typical extinction spectra of spherical silver nanoparticles (red) and silver nanoplates (blue).

- Longitudinal in-plane dipole mode at 600 nm
- Longitudinal quadrupole and transverse dipole modes at 400 nm
- Transverse out-of-plane quadrupole mode, which is characteristic of flat particles at 334 nm

The addition rate of AgNO_3 (solution B) to the nutrient one (solution A) represents an important parameter to trigger silver nanoplate morphology since the growth reaction kinetics is driven by the instantaneous concentration of reactants in solution. It has been well established [22] that in a seed-mediated growth at least two possible mechanisms are possible. In one mechanism, the surfactants form a template with a certain size. This size is dependent on the surfactant concentration and the ionic strength of the solution. When a seed is introduced into the growing solution, the surfactant-capped seed becomes part of the soft template and the growth starts by diffusing the silver atoms into the template. It is also possible that the surfactant-capped seed starts growing and as the new atoms join the nanocrystal lattice, they are protected by the surfactant monomers coming from the solution. In any case, there is a specific competition between Ostwald ripening and secondary nucleation events [15]. If AgNO_3 is added step by step, the instantaneous concentration of Ag^+ ions will always be lower than that of reducing (NaBH_4) and complexing agents (TSC): Ag^+ reduction rate will certainly depend on the concentration of species as well as on the ability of citrate to complex Ag^+ ions slowing down their reduction. It is worth noting that N_2H_4 ($E_0 = -0.230$ V) is a reductant weaker than NaBH_4 ($E_0 = -0.78$ V) and this gives a better control in the growth process. Moreover, citrate ($E_0 = -0.18$ V) mainly acts as a complexing agent of Ag^+ ions and this lowers the reduction rate of Ag nanoparticles. If the above-mentioned solutions are mixed together at a specific addition rate, seed concentration will determine the nanoplate size and their aspect ratio.

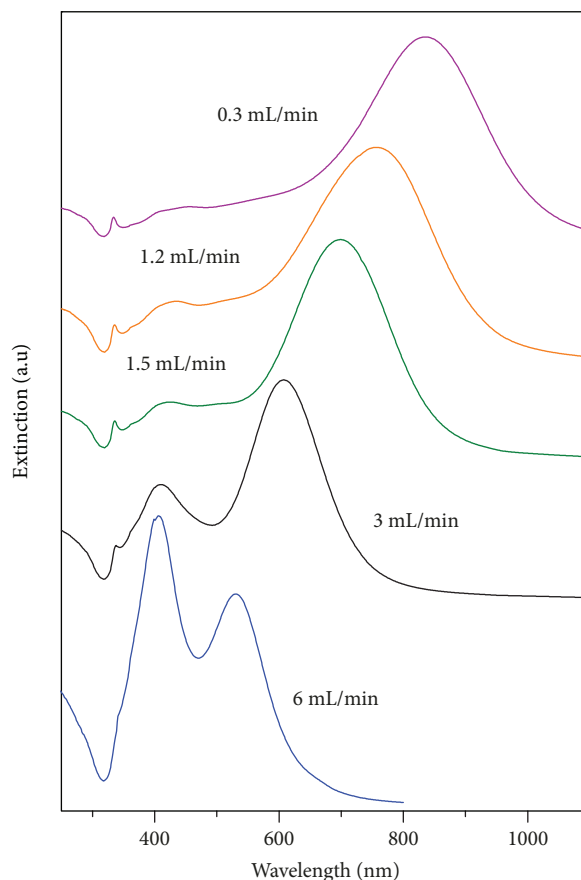
As an example, Figure 3 reports the evolution of the extinction spectra and the corresponding particle morphologies as a function of the nutrient addition rate between 6 mL/min and 0.3 mL/min. Here, we have chosen the reactor with 80 μL of initial seed colloid dispersed into 20 mL TSC and hydrazine solution. We expect a secondary nucleation which produces mostly spherical nanoparticles at high addition rates. Indeed, at addition rates above 1.5 mL/min, the overall plasmon spectrum retains a signal at 400 nm, as expected for the presence of spherical nanoparticles. Meanwhile, the competing Ostwald ripening mechanism contributes with the characteristic in-plane dipole mode, which is red shifted during the growth of the platelets. It is important to note that the signal at 400 nm is slightly shifted with respect to that obtained for the primitive seed colloid (see Figure S1 in the supporting information file). This is certainly due to the size difference between the seeds (below 20 nm) and the spherical nanoparticles grown by secondary nucleation, in which sizes can be appreciated in Figure 3(b). TEM data reported in Figure 3(b) give an idea of the situation, once the AgNO_3 nutrient solution addition rate is increased. Initially (high addition rates), the plates are quite small and the presence of spherical nuclei is evident. As the addition rate decreases, the signal at 400 nm is reduced in intensity and the longitudinal in-plane dipole mode moves towards the infrared and increases in intensity because of the plate breadth modification.

In Figure 4, we present the evolution of the longitudinal dipole mode position (localized surface plasmon resonance wavelength, λ_{LSPR}) which is related to the growing silver platelets, as a function of the nutrient solution addition time. The plot regards three different reactors (solution A) with three different concentrations of seeds. For all of them, the data show a classical saturation behaviour, which can be well presented by the empirical relation:

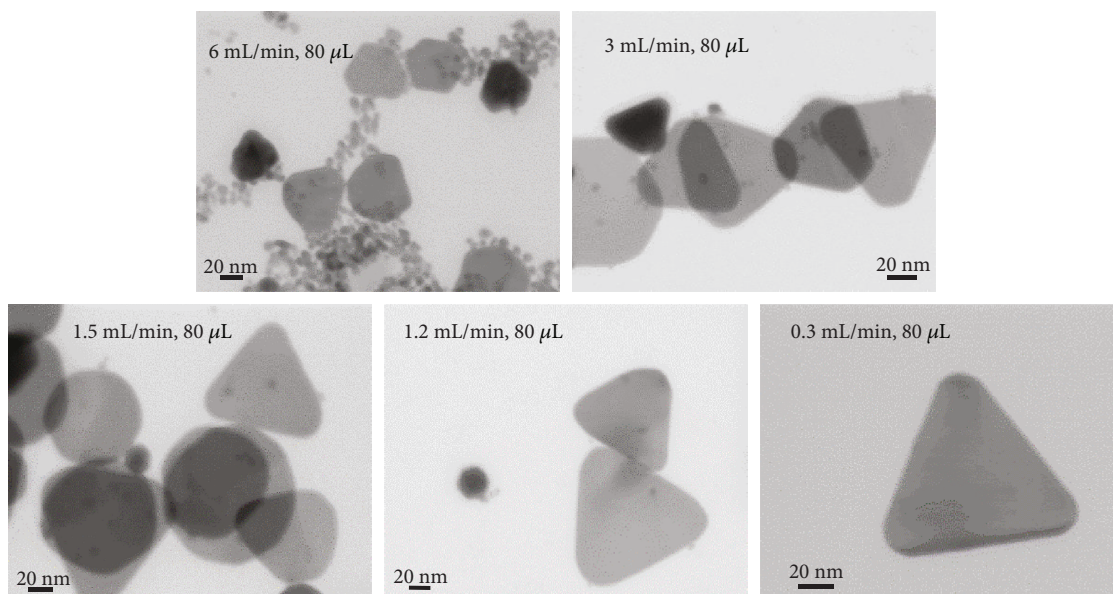
$$\lambda_{\text{LSPR}} = \lambda_{\text{sat}} + (\lambda_{\text{sat}} - \lambda_0)e^{-kt}. \quad (1)$$

We identify a saturation value λ_{sat} , a kinetic constant k , and the parameter λ_0 which represents the plasmon wavelength position at $t = 0$. λ_{sat} gives the final position of the longitudinal dipole mode, once the growth is finished. Saturation changes significantly by changing the seed concentration and reaches values above 1000 nm in the case of very diluted reactor colloids (below 80 μL). The kinetic constant k indicates how fast the growing process is. Of course, the smallest the breadth of the final particles is, the faster is the growing process, as can be seen in Table 1, where we report the fitting results obtained using equation (1).

The empirical relation in equation (1) clearly originates from a first-order kinetics. Xia et al. [23] have recently proposed the use of such a law in seed-mediated growth of colloidal metal nanocrystals. They considered that in all those cases in which the reductant is supplied in excess and the types of reagents and temperature involved are fixed, the reductant concentration remains relatively constant throughout the synthesis and so the instantaneous precursor concentration at time t can be modelled using a



(a)



(b)

FIGURE 3: (a) Plasmon signals for several platelet colloids, each obtained by changing the nutrient solution addition rate. (b) Some TEM images showing the geometric features of the silver nanoparticles obtained after different addition rates.

pseudo-first-order law. These data reflect some features of the growing mechanism.

On the other hand, it is to be considered that a seed-mediated growth (heterogeneous nucleation) is always in

competition with a homogeneous nucleation procedure. However, if we maintain the growing driving force sufficiently low, homogeneous nucleation can be prevented and heterogeneous nucleation prevalently occurs. This is the core

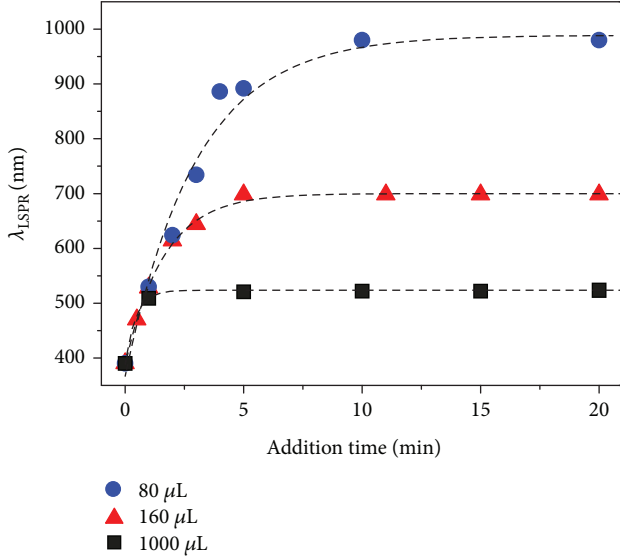


FIGURE 4: Evolution of the longitudinal dipole mode position (λ_{LSPR}) as a function of the nutrient solution addition time. The plot regards three different reactors (solution A) with three different seed concentrations.

TABLE 1: Parameters obtained as a result of the fit generated by equation (1).

	80 μL	160 μL	350 μL	1000 μL
λ_{sat}	989	700	615	524
λ_0	388	367	389	390
k (min^{-1})	0.33	0.63	1.07	2.2

of our experiment where the different batches are characterized by the number of available seeds, ready to act at the same precursor conditions. For this reason, the different kinetic constants are due to a more favourable (and then faster) environment during the growth as the initial concentration of seeds increases.

The already-mentioned differences in the saturation values indicate that the lower the seed concentration is, the greater is the average aspect ratio of the platelets grown (higher λ_{LSPR}) since the available (constant) Ag^+ ions in solution are forced to feed a lower quantity of nuclei. Of course, the time constants reflect this feeding process with values that follow a consistent trend. Figure 5 reports the extinction spectra obtained for different seed aliquots in saturation conditions (Figure 5(a)) and the relative AFM observation, once each colloid is suitably deposited onto a flat surface (Figure 5(b), see also Figure S2 in Supplementary Material). The spectral differences correspond to an increase of the aspect ratio from 3 (1000 μL) to 20 (20 μL). The plasmon resonance of the latter extends deeply into the near-infrared region.

Figure 5(b) also shows a fluctuation of the plate heights from 12 to 20 nm. This has no relevant effect on the aspect ratio since the size of the plate basal plane is at least one order

of magnitude larger than the height. We ascribe the observed fluctuation to a moderate distribution of the seed size, whose diameters should be in the range 10–20 nm, as the plasmon resonance is given at 395 nm [24].

3.2. Plasmon Resonance Sensing and the Dependence on Size and Shape. Nanoplasmonic refractometric sensing enables the detection of small refractive index (RI) changes in the dielectric medium surrounding the metal nanostructure [12, 21]. This happens through the changes of either the plasmon peak position or the intensity per refractive index units (RIU). In this work, we have defined a refractive index sensitivity S [25] as follows:

$$S = \frac{d\lambda_{\text{LSPR}}}{dn} = \frac{d\epsilon'_{\text{LSPR}}/dn}{d\epsilon'(\lambda)/d\lambda}, \quad (2)$$

where n is the refractive index of the host matrix, λ_{LSPR} is the wavelength at the maximum plasmon resonance (in-plane dipole, in our case), and ϵ' is the real part of the dielectric function of the metal constituting the nanoparticle. These measurements are generally performed by monitoring the spectral changes that occur when the plasmonic material is exposed to solutions with various well-known RIs. Literature data [26] largely report the RI sensitivity as highly dependent on the nature of the plasmonic nanoparticles (i.e., size, shape, and metal composition), so we expect to find a variety of different efficiencies in our class of silver nanoplates. For this reason, we have tested the sensitivity of our particles by controlling the surrounding refractive index with sucrose solutions prepared at different concentrations. Indeed, sucrose molecules do not interact chemically with the nanoparticles, and, at the same time, the correlation between the solution refractive index and its sucrose concentration is well established in the range between 1.333 (pure water) and 1.46 (70% w/w). Table S1 in the Supplementary Material reports the refractive index dependence on sucrose concentration [27].

Figure 6(a) reports some results after an investigation of the dipole plasmon sensitivity for some of the colloidal nanoplates under study. We have limited our study to different initial seed concentrations after a sufficiently slow AgNO_3 addition (saturation conditions). In the figure, $\Delta\lambda_{\text{max}}$ is the difference between the in-plane dipole plasmon resonance position of the nanoparticles at a given sucrose concentration (and then at a given refractive index) and that found in pure water. At first glance, it seems that the higher the platelet aspect ratio is (ratio between the breadth and the thickness of the particle), the better is the observed dipole plasmon resonance sensitivity. Indeed, it reaches $\Delta\lambda/\Delta n = 450 \text{ nm}/\text{RIU}$ for the particles prepared using 20 μL of seed solution. Some authors have observed that this trend is misleading and that the sensitivity changes are merely due to a variation of the spectral position of the plasmon resonance. In particular, Saison-Francioso et al. [28] determined an analytical expression of S in the quasistatic approximation. They found that $\Delta\lambda_{\text{LSPR}}/\Delta n$ is related to the LSPR wavelength position, the refractive index of the host matrix, and the wavelength dispersion of the real part of the dielectric function on the

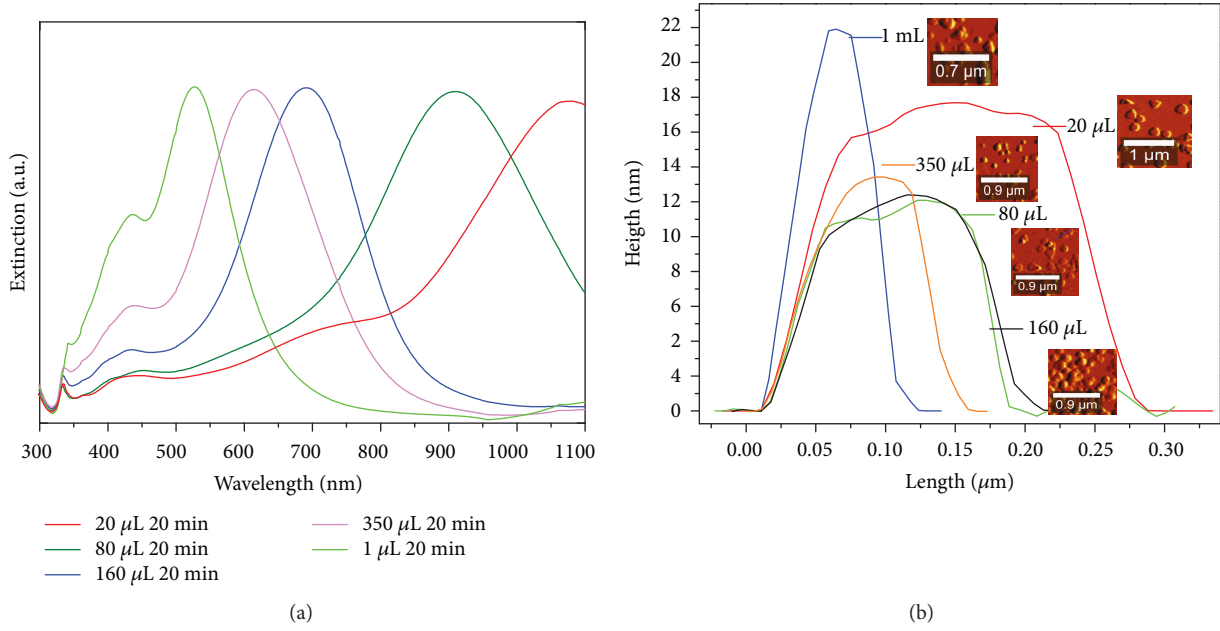


FIGURE 5: (a) Plasmon resonances in a saturation condition (very low addition rates) for several reactors, each with a different initial seed concentration. (b) The AFM profile for some of the platelets obtained.

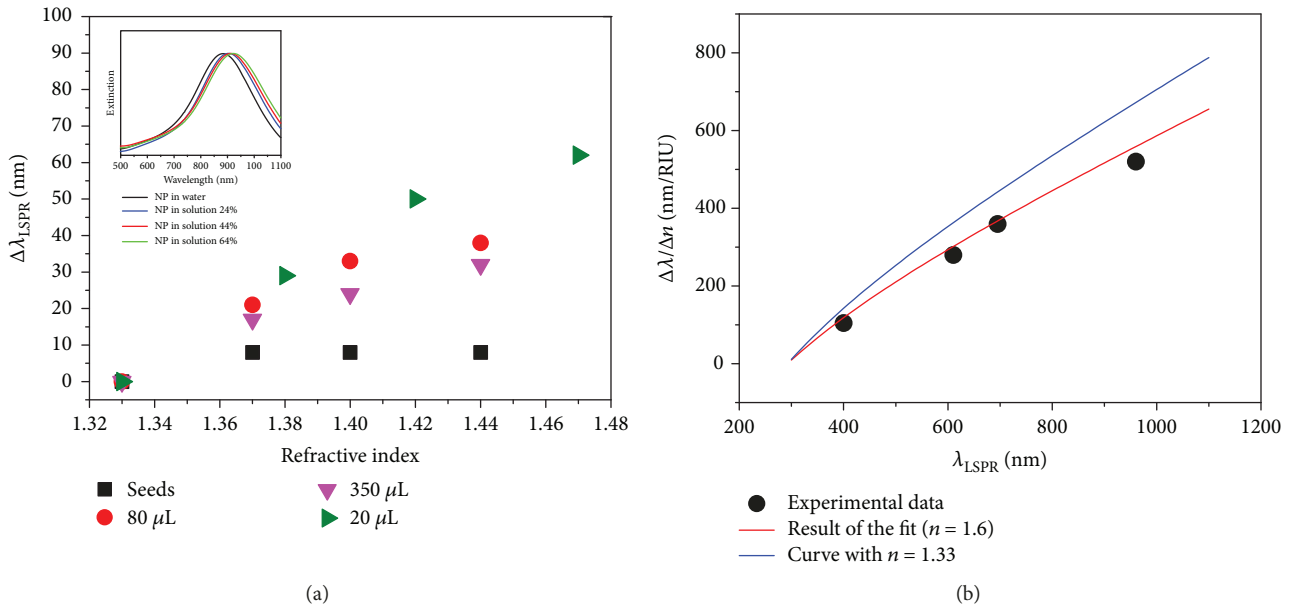


FIGURE 6: (a) Results after an investigation of the dipole plasmon sensitivity for some of the colloidal nanoplates under study. (b) Sensitivity as a function of the plasmon resonance position.

nanoparticles. Under the hypothesis of a quadratic dependence of $\epsilon'(\lambda)$ as [25]

$$\epsilon'(\lambda) = A\lambda^2 + B\lambda + C, \quad (3)$$

the final expression for S is given by

$$S = \frac{2(A\lambda_{\text{LSPR}}^2 + B\lambda_{\text{LSPR}} + C)}{n(2A\lambda_{\text{LSPR}} + B)}. \quad (4)$$

This simple correlation has been tested theoretically by comparing the analytical expression (equation (4)) with numerical simulations performed by using the well-known finite difference time domain (FDTD) method which has been used to simulate each single-plasmon resonance [28]. We want now to test such a theory with the colloidal samples previously described. We have first obtained the parameters A , B , and C by fitting $\epsilon'(\lambda)$ using equation (3) in the wavelength interval of interest (300–1500 nm) [29]. These results are reported in the Supplementary Material (Figure S3) and

have been obtained using the optical constants taken by ref. [26]. Once these parameters have been calculated, they are used to perform a final fitting procedure, using equation (3) as reported in Figure 6(b). The red curve represents a fitting with the method presented in ref. [21]. The hypothesis of Saison-Francioso et al. is respected, and a surrounding medium refractive index value of $n = 1.6$ is obtained by the fit. The value is not so far from the refractive index of water (1.33). Figure 6(b) also reports the behavior of the same curve at $n = 1.33$. We can ascribe this discrepancy to two different reasons:

- (a) A deviation from the quasistatic approximation which is evident at high λ_{LSPR}
- (b) Due to reaction by-products, the effective refractive index of the liquid surrounding the particle deviates from that of pure water

Further investigation is underway to clarify this point.

4. Conclusions

We have reported some specific experimental aspects in the synthesis of silver nanoplates by using a seed-mediated growth approach. We have described the kinetics of the platelet growth at different seed concentrations. The position of the LSPR maximum depends on both the initial seed concentration and the speed at which the seed solution is fed by the nutrient Ag^+ one. With the lowest seed concentration, in saturation conditions, we were able to obtain colloidal suspensions with dipole in plane resonances which extend beyond 1000 nm. These colloids reach plasmon sensitivity values as high as 450 nm/RIU, and each single particle has aspect ratios as high as 20. Recent literature data [30] indicate that such a sensitivity remains unchanged even after 2.5 years, a major requirement for most industrial applications. Finally, the comparison of the experimental data with an established model has demonstrated that plasmon sensitivity does not depend directly on the nanoparticle shape and aspect ratio but merely on the position of the resonance. This last consideration opens the possibility to extend further the sensitivity of AgNPTs if particle geometries and the NIR region are further explored.

Data Availability

The data used to support the findings of this study are available from the corresponding author upon request.

Conflicts of Interest

The authors declare that there is no conflict of interest regarding the publication of this paper.

Acknowledgments

The authors gratefully acknowledge the PON project Bionanotech Research and Innovation Tower (BRIT) financed by the Italian Ministry for Education, Universities and Research

(MIUR). We also acknowledge G. F. Indelli (BRIT) for the technical support.

Supplementary Materials

Figure S1: spherical particles forming during secondary nucleation and growth give a characteristic signal which is markedly shifted towards the red with respect to small silver nanoparticles. Figure S2: (a) AFM image and profile of platelets obtained with 20 μL of seed solution once the colloid is suitably deposited onto a flat surface; (b) SEM image of the same colloids. Table S1: refractive index of a sucrose aqueous solution as a function of the concentration. Figure S3: fit of $\epsilon'(\lambda)$ using equation (2) in the wavelength interval of interest (300–2000 nm). (*Supplementary Materials*)

References

- [1] D. J. Lockwood, *Noble Metal Nanoparticles: Preparation, Composite Nanostructures, Biodecoration and Collective Properties*, Springer, 2017.
- [2] D. L. Feldheim and C. A. Foss Jr, *Metal Nanoparticles: Synthesis, Characterization, and Applications*, Marcel Dekker, Inc., 2002.
- [3] F. F. Tao, *Metal Nanoparticles for Catalysis: Advances and Applications*, The Royal Society of Chemistry, 2014.
- [4] A. Trügler, *Optical Properties of Metallic Nanoparticles*, Springer International Publishing, Cham, Switzerland, 2016.
- [5] G. C. Messina, M. G. Sinatra, V. Bonanni et al., "Tuning the composition of alloy nanoparticles through laser mixing: the role of surface plasmon resonance," *Journal of Physical Chemistry C*, vol. 120, no. 23, pp. 12810–12818, 2016.
- [6] S. Zeng, D. Baillargeat, H. P. Ho, and K. T. Yong, "Nanomaterials enhanced surface plasmon resonance for biological and chemical sensing applications," *Chemical Society Reviews*, vol. 43, no. 10, pp. 3426–3452, 2014.
- [7] A. L. González, C. Noguez, J. Beránek, and A. S. Barnard, "Size, shape, stability, and color of plasmonic silver nanoparticles," *Journal of Physical Chemistry C*, vol. 118, no. 17, pp. 9128–9136, 2014.
- [8] K. Kneipp, "Surface-enhanced Raman scattering," *Physics Today*, vol. 60, no. 11, pp. 40–46, 2007.
- [9] Y. Xia, P. Yang, Y. Sun et al., "One-dimensional nanostructures: synthesis, characterization, and applications," *Advanced Materials*, vol. 15, no. 5, pp. 353–389, 2003.
- [10] J. Yin, Y. Zang, C. Yue et al., "Ag nanoparticle/ZnO hollow nanosphere arrays: large scale synthesis and surface plasmon resonance effect induced Raman scattering enhancement," *Journal of Materials Chemistry*, vol. 22, no. 16, pp. 7902–7909, 2012.
- [11] R. Fiorenza, M. Bellardita, L. D'Urso, G. Compagnini, L. Palmisano, and S. Scirè, "Au/TiO₂-CeO₂ catalysts for photocatalytic water splitting and VOCs oxidation reactions," *Catalysts*, vol. 6, no. 8, p. 121, 2016.
- [12] M. Xiao, R. Jiang, F. Wang, C. Fang, J. Wang, and J. C. Yu, "Plasmon-enhanced chemical reactions," *Journal of Materials Chemistry A*, vol. 1, no. 19, pp. 5790–5805, 2013.
- [13] X. Zhou, G. Liu, J. Yu, and W. Fan, "Surface plasmon resonance-mediated photocatalysis by noble metal-based composites under visible light," *Journal of Materials Chemistry*, vol. 22, no. 40, pp. 21337–21354, 2012.

- [14] L. Guo, J. A. Jackman, H. H. Yang, P. Chen, N. J. Cho, and D. H. Kim, "Strategies for enhancing the sensitivity of plasmonic nanosensors," *Nano Today*, vol. 10, no. 2, pp. 213–239, 2015.
- [15] A. J. Haes and R. P. Van Duyne, "A nanoscale optical biosensor: sensitivity and selectivity of an approach based on the localized surface plasmon resonance spectroscopy of triangular silver nanoparticles," *Journal of the American Chemical Society*, vol. 124, no. 35, pp. 10596–10604, 2002.
- [16] I. Pastoriza-Santos and L. M. Liz-Marzán, "Colloidal silver nanoplates. State of the art and future challenges," *Journal of Materials Chemistry*, vol. 18, no. 15, pp. 1724–1737, 2008.
- [17] X. Liu, L. Li, Y. Yang, Y. Yin, and C. Gao, "One-step growth of triangular silver nanoplates with predictable sizes on a large scale," *Nanoscale*, vol. 6, no. 9, pp. 4513–4516, 2014.
- [18] W. Niu, L. Zhang, and G. Xu, "Seed-mediated growth of noble metal nanocrystals: crystal growth and shape control," *Nanoscale*, vol. 5, no. 8, pp. 3172–3181, 2013.
- [19] R. Zong, X. Wang, S. Shi, and Y. Zhu, "Kinetically controlled seed-mediated growth of narrow dispersed silver nanoparticles up to 120 nm: secondary nucleation, size focusing, and Ostwald ripening," *Physical Chemistry Chemical Physics*, vol. 16, no. 9, pp. 4236–4241, 2014.
- [20] C. F. Bohren and D. R. Huffman, *Absorption and Scattering of Light by Small Particles*, Wiley, 1998.
- [21] X. Y. Zhang, A. Hu, T. Zhang et al., "Self-assembly of large-scale and ultrathin silver nanoplate films with tunable plasmon resonance properties," *ACS Nano*, vol. 5, no. 11, pp. 9082–9092, 2011.
- [22] B. Nikoobakht and M. A. El-Sayed, "Preparation and growth mechanism of gold nanorods (NRs) using seed-mediated growth method," *Chemistry of Materials*, vol. 15, no. 10, pp. 1957–1962, 2003.
- [23] Y. Xia, K. D. Gilroy, H. C. Peng, and X. Xia, "Seed-mediated growth of colloidal metal nanocrystals," *Angewandte Chemie International Edition*, vol. 56, no. 1, pp. 60–95, 2017.
- [24] S. Agnihotri, S. Mukherji, and S. Mukherji, "Size-controlled silver nanoparticles synthesized over the range 5–100 nm using the same protocol and their antibacterial efficacy," *RSC Advances*, vol. 4, no. 8, pp. 3974–3983, 2014.
- [25] M. M. Miller and A. A. Lazarides, "Sensitivity of metal nanoparticle surface plasmon resonance to the dielectric environment," *The Journal of Physical Chemistry B*, vol. 109, no. 46, pp. 21556–21565, 2005.
- [26] Y. Liu, S. Pedireddy, Y. H. Lee et al., "Precision synthesis: designing hot spots over hot spots via selective gold deposition on silver octahedra edges," *Small*, vol. 10, no. 23, pp. 4940–4950, 2014.
- [27] E. Martinsson, M. M. Shahjamali, K. Enander et al., "Local refractive index sensing based on edge gold-coated silver nanoprisms," *Journal of Physical Chemistry C*, vol. 117, no. 44, pp. 23148–23154, 2013.
- [28] O. Saison-Francioso, G. Lévêque, R. Boukherroub, S. Szunerits, and A. Akjouj, "Dependence between the refractive-index sensitivity of metallic nanoparticles and the spectral position of their localized surface plasmon band: a numerical and analytical study," *Journal of Physical Chemistry C*, vol. 119, no. 51, pp. 28551–28559, 2015.
- [29] P. B. Johnson and R. W. Christy, "Optical constants of the noble metals," *Physical Review B*, vol. 6, no. 12, pp. 4370–4379, 1972.
- [30] S. Biswas and P. Kumbhakar, "Refractive index and temperature sensing in anisotropic silver nanostructures with stable photo-physical properties," *Applied Physics A: Materials Science & Processing*, vol. 124, no. 1, p. 6, 2018.



Hindawi
Submit your manuscripts at
www.hindawi.com

